climate

MDPI

Article

Prognosis for Brazilian Agricultural Production: The Impact of Drought-Sensitive Crops on the Climate

João Lucas Della-Silva [1], Fernando Saragosa Rossi [2], Damien Arvor [3], Gabriela Souza de Oliveira [2], Larissa Pereira Ribeiro Teodoro [2], Paulo Eduardo Teodoro [2,*], Tatiane Deoti Pelissari [1], Wendel Bueno Morinigo [1] and Carlos Antonio da Silva Junior [1]

[1] Universidade do Estado de Mato Grosso (UNEMAT), Campus de Sinop, Sinop 78550-000, Brazil; joao.lucas1@unemat.br (J.L.D.-S.); td.pelissari@unesp.br (T.D.P.); wendelbmorinigo@hotmail.com (W.B.M.); carlosjr@unemat.br (C.A.S.J.)
[2] Universidade Federal de Mato Grosso do Sul (UFMS), CPCS, Chapadão do Sul 79560-000, Mato Grosso do Sul, Brazil; gabriela_souza@ufms.br (G.S.O.); ffernando_rossi@ufms.br (F.S.R.); larissa._ribeiro@ufms.br (L.P.R.T.); paulo.teodoro@ufms.br (P.E.T.)
[3] Centre National de la Recherche Scientifique, UMR 6554 LETG, Université Rennes 2, 35043 Rennes, France; damien.arvor@univ-rennes2.fr
* Correspondence: carlosjr@unemat.br

Abstract

The northern part of the state of Mato Grosso is located at the intersection of large-scale agricultural production and the Amazon, a tropical biome of great importance for ecosystem services and biodiversity. Agricultural production activities interact with natural capital, among other factors, in land use and in biogeochemical cycles of water and carbon. In this study, we sought to use remote sensing at the regional level to diagnose and spatialize the contribution of agricultural activity to dry areas. Using carbon dioxide orbital models, land use classification techniques, the Standardized Precipitation Index (SPI), and Pettitt and Mann–Kendall statistics, the variables were compared spatially for the biogeographic boundary of the Amazon in Mato Grosso in two distinct time frames: (i) over the crop years of the CO_2 efflux model (2020 to 2023), and (ii) over the years 2008 to 2023, with consolidated data from the MODIS sensor system. The hot and cold spots analysis reinforces the correlation of carbon variables to land use; the drought index suggests a spatial correlation to forest loss, where more intense agricultural activity favors drought and inhibits moderate rainfall, and in turn is linked to the amount of forest in the context of intense continentality. Temporally, the statistical diagnosis highlights abrupt changes in 2011, 2013, and 2019, restate the complex relation of tropical forest and biogeochemical cycles, above all with carbon dioxide.

Keywords: remote sensing of the environment; soybeans; biogeochemical cycles

Academic Editor(s): Name

Received: 14 January 2026
Revised: 13 February 2026
Accepted: 18 February 2026
Published: date

1. Introduction

The Brazilian economy relies heavily on commodity exports, particularly soybeans, (*Glicine max* L. Merrill) [1], mainly exported in grain form [2]. This production is mainly carried out in the Central West region of the country, highlighting the state of Mato Grosso [3–5], which, with its geographical conditions and technological development in genetic improvement, allows efficient cultivation in extensive areas of crops in the region [6–9].

In a context prior to agricultural occupation, the southern Amazon biome also occurs in Mato Grosso, with its intersection exactly in the north of the state. Historically, the biome has been subjected to intense deforestation, which began with state policies for the occupation of native forest areas in the 1960s [10], and advanced with economic practices of using wood, mining, livestock farming and finally with the dominance of agriculture [11–13]. This great productive capacity makes Brazil a major grain exporter.

While economic development stresses the natural capital of a biome highly sensitive to anthropization, the climate conditions of the Brazilian Midwest are dependent on ecosystem services from the Amazon rainforest [14–16]. The geomorphological structure of the American continent, with the presence of the Andes, combined with the phenomenon of 'flying rivers', due to the evapotranspiration of the tropical forest, creates a unique condition that contains the desertification of a region prone to such [17].

The retreat of Amazonian evergreen forests, transformed into agricultural and livestock areas, potentializes desertification, since forests are the main component of the deceleration of the desertification process [18]. Climatic unfeasibility would significantly impact precipitation and, consequently, local biodiversity and, correlated to changes in productive performance in this crop, due to atmospheric conditions of CO_2 and temperature, in productive capacity [19,20]. Therefore, it would affect the Brazilian economy, as well as food security for those who consume its products [21,22].

When dealing with dynamics on land use, orbital data on Earth's surface reflectance and remote sensing techniques are highlighted in contemporary science and are suitable for this purpose [23]. Moreover, combining climatic and biogeochemical aspects increases the importance of such methods. Analyses of carbon balance, climatological aspects, occupation by agricultural crops, or more specifically on soybeans in Brazil adhere to and are consecrated with the use of remote sensing [24].

In the context of remote sensing, the capability of regionalized analyses of environmental dynamics is sometimes limited to estimates, especially when it comes to specific target classification and carbon studies [25,26]. Despite the great potential in mapping extensive cultivation areas, the analysis of floristics is still limited, where the spectral mixing effect exemplifies part of the limitations. To achieve greater reliability in the results, in situ remote sensing techniques are necessary to provide reliable results to the models applied at the orbital level [27–29].

Among the in situ instruments, soil CO_2 efflux analysis observes part of the dynamics between carbon stocks, which is related to the type of surface cover [27,30]. Infrared gas analyzer (IRGA) instruments then provide data for building models with orbital data to estimate at a regional level, results for the same variable [31]. Thus, the construction of such a model gathers new capabilities for sensing and the contribution of science to environmental diagnosis [32].

To contextualize the dynamics of CO_2 efflux, carbon emissions are correlated with biotic stock, which implies the capacity to absorb atmospheric carbon [19]. Therefore, a larger photosynthetic biosphere increases the presence of organic carbon, characterizing a coverage with greater CO_2 emissions [33]. In contrast, different carbon dynamics are expected over extensive livestock farming and crop areas, which, with lower biotic stock capacity, have limited carbon stocks in soil and affect the overall condition of this element among stocks [34,35].

In short, anthropization (and more specifically, soybean cultivation) acts on the biogeochemical cycles of water and carbon, on its impact and its consequences on the regional climate [36,37]. Such dynamics adhere to remote sensing, which, with appropriate methods, finds results and diagnoses that permeate and contribute to environmental science and agriculture, especially in a bias with the potential to improve yields, rather than expanding arable areas [6,38].

Understanding spatialized carbon and water cycles, and their correlation to human activity with remote sensing may rely on a robust background of variables, given the complexity of biogeochemical cycles and their relation to anthropization. Our hypothesis is that remotely sensed data of carbon and drought can be spatially correlated to land use dynamics, namely the agricultural expansion over the southern Amazonian rainforest. Since the anthropization means loss of evergreen forest and then drought, the soybean cultivation is affected by alterations on precipitation regime [20]. Given the context presented, this work will analyze the predicted impact of the expansion of soybean areas within the biogeographic limit of the Amazon based on orbital models for estimating carbon balance (GPP, CO_2Flux, FCO_2), drought and land use for the agricultural calendars from 2020 to 2023.

2. Materials and Methods

In this work, the potential spatial relationship between drought and the expansion of arable areas will be verified by using remote sensing and geoprocessing data and techniques held on the Google Earth Engine (Mountain View, CA, USA) platform [39].

2.1. Study Site

The region of interest refers to the biogeographic limit of the Amazon within the political boundary of the state of Mato Grosso, Brazil, placed from 09º00′ to 18º00′ S and 49º00′ to 61º00′ W (Figure 1). With an area of about 661 thousand km² and covered by 92 municipalities, the climate in the region is super humid tropical monsoon, with high average annual temperature above 24 °C and high rainfall (2000 mm year^{-1}); tropical, with summer rains and dry winter, characterized by averages of 23 °C on the plateau, which according to the Köppen–Geiger classification are "Am" (monsoon climate) and "Aw/As" (tropical climate with dry season).

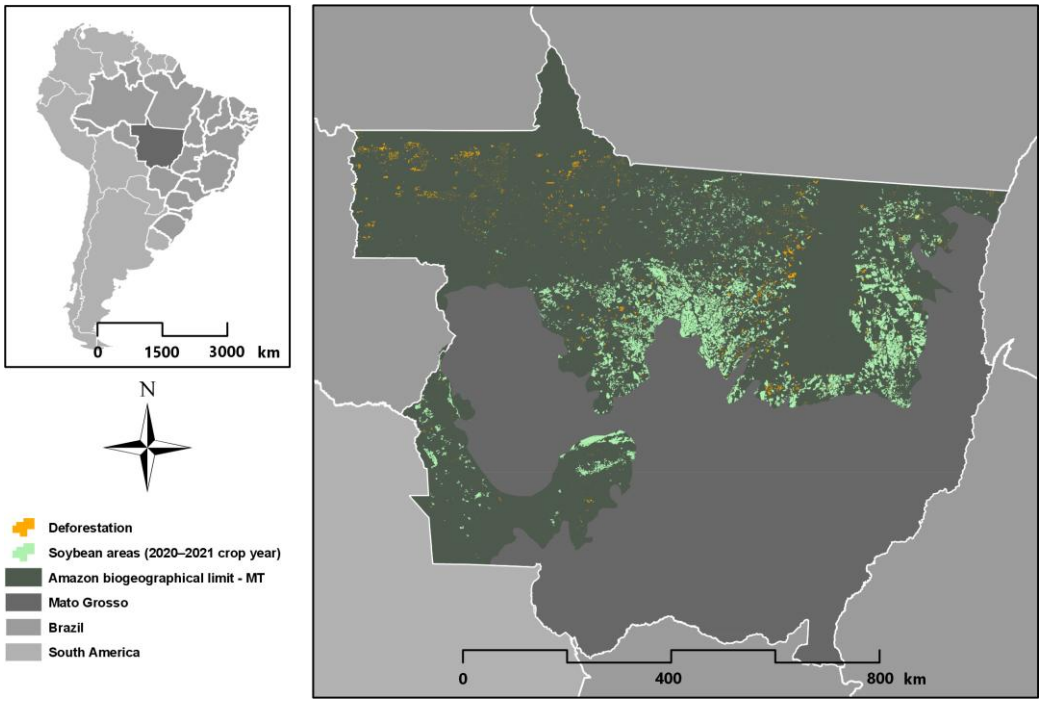

Figure 1. Study area: biogeographic limit of the Amazon in the state of Mato Grosso and anthropization.

2.2. Land Use

2.2.1. Soybean Cultivation Areas

The definition of the soybean class for the study area is based on SojaMaps data [40]. This is a product generated from the analysis of orbital surface reflectance images from MODIS sensors (on board the TERRA and AQUA systems), considering agronomic conditions associated with the temporal context [41].

Specifically, the process relies on the entire soybean crop cycle imaging, from sowing to harvesting. MODIS orbital images are acquired, and a time series is established. Among the numerous processes for generating the product, soybean areas depend on the classification based on the vegetation indexes Perpendicular Crop Enhancement Index (*PCEI*—Equation (2)), based on the maximum and minimum values of the Perpendicular Vegetation Index (*PVI*—Equation (1)) for the series. The maximum *PVI* values are observed in the period of maximum development of the soybean crop, while the minimum values are observed in the period prior to the planting or emergence. Finally, the highest *PCEI* values are classified as soybean.

$$PVI = \frac{1}{\sqrt{1+a^2}} \times (\rho_{NIR} - a \times \rho_{RED} - b) \quad (1)$$

$$PCEI = g \times \frac{(Max\ PVI + S) - (Min\ PVI + S)}{(Max\ PVI + S) + (Min\ PVI + S)} \quad (2)$$

where

ρ_{NIR} is the near-infrared band reflectance.

ρ_{RED} is the red band reflectance.

a is the soil line slope.

b is the soil line gradient.

S is the enhancement coefficient (10^2).

b is the gain factor (10^2).

In subsequent steps, geo-object-oriented analysis and machine learning vectorization are performed, supported by higher spatial resolution orbital images from the OLI/Landsat-8 and MSI/Sentinel-2 sensor systems. The use of machine learning, specifically the Random Forest model, smooths and refines the results of the soybean maps [40].

2.2.2. Forest Degradation

To detect changes in the forest class, the Normalized Difference Fraction Index (NDFI) was applied [42]. Through this model, the proportions of the classes on each pixel are determined, supported by the Linear Spectral Unmixing (LSU) (Equations (3) and (4)). This algorithm aims to estimate the proportion of components, such as soil, shade, healthy vegetation and non-photosynthetic vegetation of each pixel, from the spectral response in the different spectral bands of the OLI, generating the fraction images [43].

$$R_n = \sum_{i=1}^{n} F_i\, R_{i,b} + \varepsilon_b \quad (3)$$

$$\sum_{i=1}^{n} F_i = 1 \quad (4)$$

where:

R_b is b band reflectance.

$R_{i,b}$ is the reflectance for user i, in spectral band b.

F_i is the fraction of endmember i.

ε_b is the residual error for each band.

The LSU error for each image pixel is estimated by mean squared error (*MSE*) (Equation (5)):

$$MSE = \left[n^{-1} \sum_{b=1}^{n} \varepsilon_b \right]^{1/2} \quad (5)$$

Finally, the model will then be applied to each image of each spectral band using the seven OLI bands and endmembers selected in the image itself (Equation (6)).

$$NDFI = \frac{GV_{Shade} - (NPV + Soil)}{GV_{Shade} + NPV + Soil} \quad (6)$$

where:

NPV is non-photosynthetic vegetation.

GV_{shade} is the shade-normalized green vegetation (*GV*) fraction (Equation (7)).

$$GV_{Shade} = \frac{GV}{100 - Shade} \quad (7)$$

NDFI values range from −1 to 1, with intact forests having high values (close to 1) due to the combination of high SV (i.e., high SV content and canopy shade) and low VFN and soil values. As forests become degraded, *NPV* and soil fractions increase due to decreasing canopy cover, reducing *NDFI* values relative to intact forests [44]. An empirical decision tree model for deforestation detection is also proposed, which generally translates the biophysical responses of vegetation (Figure 2).

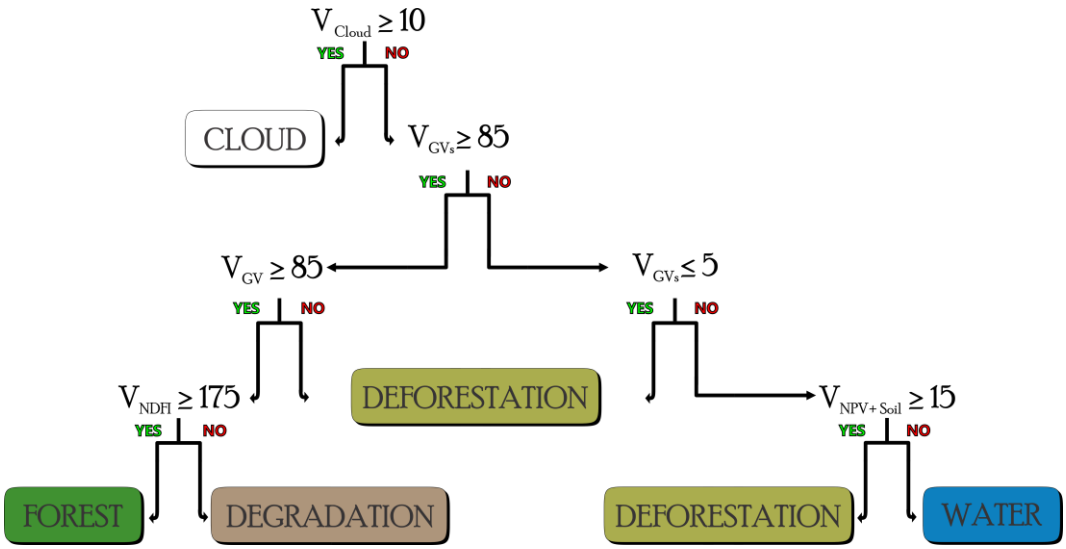

Figure 2. Empirical decision tree used for classifying deforestation and forest degradation [44]. NDFI variable was rescaled to 0–200, meaning that VNDFI ≥ 175 translates to VNDFI ≥ 0.75 formatting.

In addition to these values for deforestation data, PRODES (Sistema de Monitoramento do Desmatamento na Amazônia Legal) data, from INPE (Instituto Nacional de Pesquisas Espaciais) was used, based on August 2008 (Soy Moratorium agreement) to July 2023. Then, the deforested areas in these years will be combined to verify the areas (polygons) converted from forest-soybean and forest-pasture-soybean for all municipalities that are part of the Amazon in the state of Mato Grosso.

2.3. Carbon Dioxide Dynamics

2.3.1. Carbon Dioxide Uptake

Based on the relationship between land cover and CO2, surface reflectance data from orbital sensors can provide spatialized data for carbon-related variables. GPP MODIS [45] and the CO_2Flux [46] model will be used. For the last one, environmental [47] and spectral rates [25] of input data will be considered.

Gross Primary Production (GPP)

The MOD and MYD17A2 products are cumulative composites of gross primary productivity values, based on the concept of the efficient use of solar radiation by vegetation (ε). In this logic, primary production is linearly related to absorbed photosynthetically active radiation (APAR) (Equation (8)). APAR can be calculated as the product of the incident photosynthetically active radiation (PAR), in the visible spectral range of 0.4–0.7 μm, assumed to be 45% of the total incident solar radiation, and the fraction of photosynthetically active radiation absorbed by the vegetation cover ($FPAR$) [45].

$$GPP = \varepsilon \times PAR \times FPAR \quad (8)$$

One of the biggest challenges in using such models is obtaining the light use efficiency "ε" over a large area, due to its dependence on environmental factors and the vegetation itself. One of the solutions consists of relating "ε" according to its maximum value (ε_{max}), the environmental contributions synthesized by the minimum air temperature ($T_{minscalar}$) and the water state in the vegetation (water vapor pressure deficit—VPD) (Equation (9)) [48].

$$\varepsilon = \varepsilon_{max} \times T_{minscalar} \times VPD_{scalar} \quad (9)$$

In this study, MODIS GPP (Gross Primary Production), version 5.0, with composition between the years 2008 and 2021 will be used. The pixel values referring to the digital numbers of the MODIS images will be converted into biophysical values (Kg C m^{-2}) by multiplying by the scale factor 0.0001 [49] (Equation (10)). *GPP* values will also be transformed from 8 day cumulative values to 8 day average values and converted from Kg C m^{-2} day^{-1} to g C m^{-2} day^{-1}. Note that *GPP* only admits positive values, since it accumulates every metabolic outcome of photosynthesis.

$$GPP\ (\text{g C m}^{-2}\ \text{d}^{-1}) = \frac{Biophysical\ Pixel\ (K\text{g C m}^{-2}\ \text{day}^{-1})}{8} \quad (10)$$

CO_2Flux

The estimation of carbon flux between soil, biotic and atmospheric stocks is highly related to land use; therefore, it can be estimated from reflectance data. Based on a component that represents vegetative vigor ($NDVI$—Equation (11)) and another for leaf water content (PRI—Equation (12)), CO_2Flux (Equation (14)) is an index that expresses such a condition [46]. Since there is a high dependence on land use, the model must be adjusted to environmental conditions [47], as well as adapted for input with multispectral orbital data, i.e., it was validated by comparing hyperspectral and multispectral values of the same method ($R^2 = 0.78$) at the same context [25]. Positive values refer to carbon emission from soil to the atmosphere, and negative values mean the carbon uptake by photosynthetic organisms. To obtain consistent results, the Photochemical Reflectance Index is scaled for positive values (Equation (13)).

$$NDVI = \frac{\rho_{NIR} - \rho_{RED}}{\rho_{NIR} + \rho_{RED}} \quad (11)$$

$$PRI = \frac{\rho_{BLUE} - \rho_{GREEN}}{\rho_{BLUE} + \rho_{GREEN}} \quad (12)$$

$$sPRI = \frac{1 + PRI}{2} \quad (13)$$

$$CO_2Flux\ (\mu mol\ m^{-2}\ s^{-1}) = 13.63 - 66.207 \times (NDVI \times sPRI) \quad (14)$$

where:

ρ_{NIR} is the near-infrared band reflectance.
ρ_{RED} is the red band reflectance.
ρ_{BLUE} is the blue band reflectance.
ρ_{GREEN} is the green band reflectance.

2.3.2. Carbon Dioxide Emission

Soil CO_2 efflux is a component of carbon dynamics. PLSR models will be used to estimate carbon dioxide efflux [26] for the soybean class, based on the MODIS sensor reflectance data (Equation (15)). In addition to the MODIS surface reflectance data, the surface temperature (LST) and soil moisture inputs will be based on the MOD11A1 V6.1 [50] and the SPL3SMP_E.006 SMAP L3 [51–53] orbital data, respectively.

$$FCO_2 = M_s \cdot 0.1658 + T_s \cdot 0.1500 + \rho_B \cdot 16.21 + \rho_G \cdot 2.04 + \rho_R \cdot (-34.34) + \rho_{NIR} \cdot 2.08 \quad (15)$$

where:

M_s is the soil moisture.
T_s is the soil temperature.
ρ_{NIR} is the near-infrared band reflectance.
ρ_{RED} is the red band reflectance.
ρ_{BLUE} is the blue band reflectance.
ρ_{GREEN} is the green band reflectance

2.4. Standardized Precipitation Index

The Standardized Precipitation Index (SPI) [54] allows a diagnosis of drought severity, where the onset and duration of the drought are perceived. Furthermore, based on an analysis with an appropriate time scale, it is possible to analyze the frequency of drought events.

The SPI seeks to quantify the deficit or excess of rainfall on different time scales and will be calculated on an annual scale (SPI-12) for the study area for the years 2008 to 2023 to identify drought events in the historical time series. The calculation (SPI) is performed based on the total accumulated rainfall records over 20 years, adjusted to a probability distribution function. The function is transformed into a normal probability distribution function, thus adjusting the average SPI value of a given location and period to zero.

To determine the SPI, the Gamma distribution calculation will initially be used, which was defined by the probability density function (PDF—Equation (16)).

$$f(x) = \frac{1}{\Gamma(a)\beta^a} x^{a-1} e^{-\frac{x}{\beta}} \quad (16)$$

where:

$\alpha > 0$ (α) shape parameter (dimensionless).
$\beta > 0$ (β) scale parameter (mm).
$x > 0$ (x) total rainfall (mm).
Γ (α) is the Gamma function (Equation (17)).

$$\Gamma(a) = \int_0^\infty x^{a-1}e^{-x}dx \quad (17)$$

All parameters and the gamma PDF will be adjusted to the frequency distribution of accumulated rainfall using remote sensing data. The parameters α and β will be calculated from the estimated Gamma probability density function for each of them at the scale. The parameters α and β will be estimated using the maximum likelihood method (MLM), which is the most appropriate method [55]. To find the cumulative probability (Equation (18)) of an observed rainfall event for the adopted scale, the parameters α and β were calculated.

$$F(x) = \int_0^x f(x)dx = \frac{1}{\Gamma(a)\beta^a}\int_0^x x^{a-1}e^{-\frac{x}{\beta}}dx \quad (18)$$

Based on the annual SPI values for the Mato Grosso Amazon, the wet and dry periods will be classified, in detail extremely wet (≥2.00), very wet (1.5 to 1.99), moderately wet (1.00 to 1.49), close to normal (0.99 to −0.99), moderately dry (−1.00 to −1.49), very dry (−1.50 to −1.99) and extremely dry (≤−2.00) [54].

Therefore, CHIRPS data will be used for precipitation estimation [56]. It is a product combining pentadal precipitation climatology, quasi-global geostationary TIR satellite observations from the CPC and the National Climatic Data Center (NCDC) [57], precipitation fields from the NOAA Climate Forecast System (CFSv2) atmospheric model [58], and in situ precipitation observations [59]. In the first stage of the study, these products will be used due to the lack of temporal data from in situ stations and because they have been available since 1981 to the present, with a spatial resolution of 0.05° (±5.3 km) and monthly, pentadal and decadal temporal resolution for the entire globe [60]. In the second stage, it is expected that meteorological stations will be acquired to monitor the areas identified as dry zones. To evaluate, compare and reflect the characteristics of the spatial distribution of precipitation and SPI, the IDW-Inverse Distance Weighting data interpolation method will be used [61].

2.5. Statistics

To identify trends throughout the time series (2008–2023) of each variable, Pettitt's test will be used. This nonparametric test allows us to confirm the stationarity of the historical series, that is, except for random fluctuations, the observations are invariant with respect to the chronology of their occurrences. The test will use two samples X_1,..., X_t and X_{t+1},...., X_T which will belong to the same population. $U_{t,T}$ statistics count the number of times a member of the 1st sample is greater than a member of the 2nd sample (Equation (19)).

$$U_{t,T} = U_{t-1,T} + \sum_{j=1}^{T} sgn(X_i - X_j) \qquad \text{for } t = 2,\ldots,T \quad (19)$$

where:

$sgn\ (x) = 1$ when $x > 0$.

$sgn\ (x) = 0$ when $x = 0$.

$sgn\ (x) = -1$ when $x < 0$.

$U_{t,T}$ is calculated for values $1 < t < T$, and the Pettitt test statistic $k(t)$ is given by (Equation (20)):

$$k(t) = MAX_{1 \ll t \ll T}\left|U_{t,T}\right| \quad (20)$$

Using Pettitt's test, the point at which a sudden change in a time series is found, and the significance of this change (p) is given by (Equation (21)):

$$p \cong 2exp\left\{\frac{-6k(t)^2}{(T^3+T^2)}\right\} \quad (21)$$

The point of abrupt change is t where the maximum of *k(t)* occurs. The critical values of *K* are given by (Equation (22)):

$$K_{crit} = \pm\sqrt{\frac{-\ln(\frac{p}{2})(T^3+T^2)}{6}} \quad (22)$$

To analyze the trend of the time series of variables, the Mann–Kendall test was applied (Eq. 23 – 25).

$$Z_{MK} = \frac{S-1}{\sqrt{Var(S)}}, when\ S > 0 \quad (23)$$

$$Z_{MK} = 0, when\ S = 0 \quad (24)$$

$$Z_{MK} = \frac{S+1}{\sqrt{Var(S)}}, when\ S < 0 \quad (25)$$

where:

Z_{MK} is the Z-index of the Mann–Kendall test.

S is the "score" statistic.

$Var(S)$ is the variance of statistic S.

2.6. Analysis of Hot and Cold Spots

The "undulating clusters" parameter is used to evaluate the spatial arrangement of the analyzed spatial variable resources. In this case, the values converted from raster to vector values of the variables CO2Flux, GPP, SPI, areas with soybeans, pastures, forests and deforestation will be selected. The number in the selected field was used to determine the clustering, and then, the tool was used to dimension the hot and cold spot areas. For this, the Getis-Ord Gi* statistics were calculated (Equation 26) [62] for each feature in the dataset. The resulting z-score and p-value will be calculated, and information will be obtained where there are spatially clustered data with high or low values. From the "Find High Incidence Values" tool, favorable patterns were calculated based on the characteristics of the input data and will automatically apply false discovery rate (FDR) corrections, analyzing each feature in the context of neighboring data.

$$Gi^*(\mathrm{d}) = \frac{\sum_{j=1}^{n} W_{ij}(d)x_j}{\sum_{j=1}^{n} x_j} \quad (26)$$

3. Results

3.1. Soil CO_2 Efflux Application

Based on the soybean areas mapped for the 2020–21 to 2022–23 crop years, the soil carbon efflux (FCO_2) model with the best adherence, represented the actual variability of soybean crops in the study area (HYS + LYS without carbon), which also determined the source of the input data (MODIS sensor system) for acquisition [26]. Also noteworthy in this regard are the spatial and spectral resolutions that are most suitable for this purpose (Fig. 3).

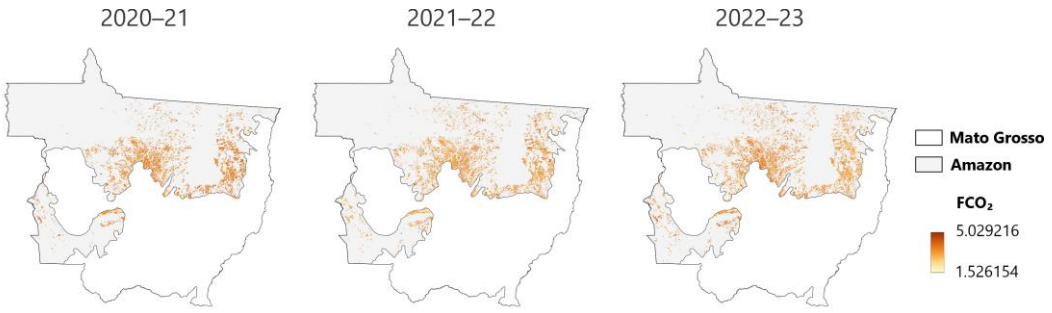

Figure 3. Orbital model of FCO_2 [μmol m^{-2} s^{-1}] over soybean areas from 2020–21 to 2022-23 crop years. The FCO_2 model for soybean areas decouples the soil carbon flow to the atmosphere from the total carbon cycle and its contribution to climatic outcomes.

The biophysical values estimated with the *FCO₂* model are feasible, and the statistical tests presented below reaffirm this determination. It should be noted that the model was applied only within the boundaries of soybean areas, and therefore, the areas of each crop year were conditioning factors for the application of the model.

3.2. Carbon and Drought Temporal Analysis

GPP, CO_2Flux and SPI Through Crop Years

The spatial analysis of carbon orbital products (GPP and CO_2Flux) and the drought severity index during harvests showed few changes, but with conclusions related to the dynamics of area conversion. Based on PRODES data, presented in the context of drought severity, it reveals that the pattern of anthropized areas advancing on the native Amazon rainforest has an impact in the short term (Figures 4 and 5).

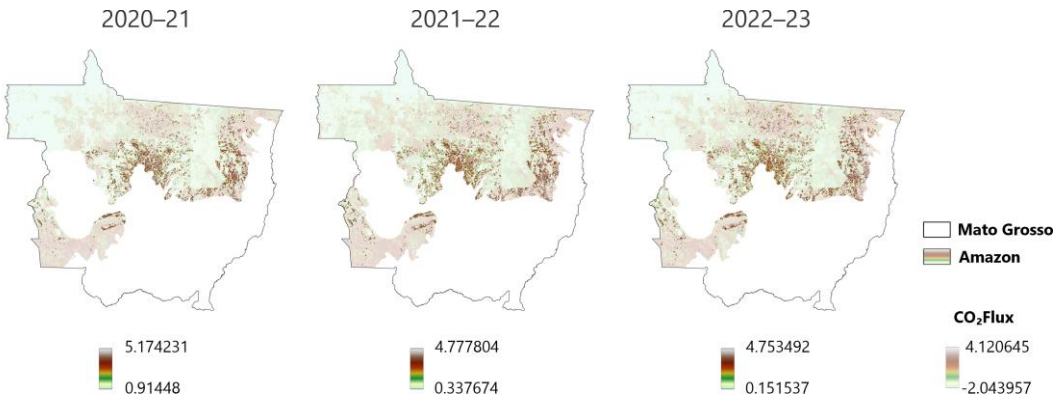

Figure 4. CO_2Flux [μmol m^{-2} s^{-1}] over soybean areas from 2020–21 to 2022-23 crop years. The orbital estimation soil-atmospheric carbon flow depends on vegetation spectral models and is closely related to land use.

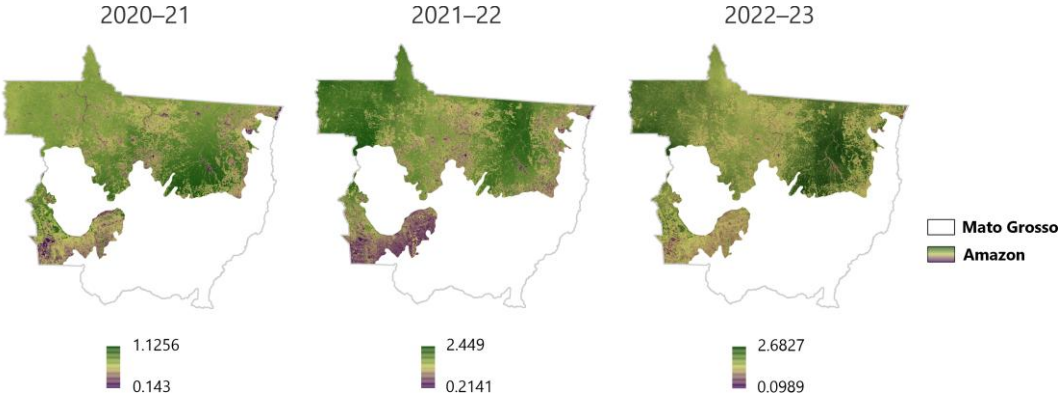

Figure 5. Annual cumulated GPP [kg C m^{-2}] over Mato Grosso Amazon from 2020–21 to 2022-23 crop years. The light-use efficiency by photosynthetically active vegetation expresses the carbon uptake, and then, the soil carbon pool.

To analyze the severity of drought on the crops under study, the index related to this condition (SPI) was calculated over the interval of the crops analyzed, still based on annual temporality (SPI-12), that is, the years 2020 to 2023. The result of the spatialized SPI (Figure 6) is notably related to precipitation and macroclimatic dynamics. Years with higher rainfall impact severity, and the cyclical nature of climatic events such as El Niño are related to the effect of drought. What this result reveals is the small or zero contribution of agricultural expansion, i.e., as a vector of effect on the climate, towards an increase in the drought index.

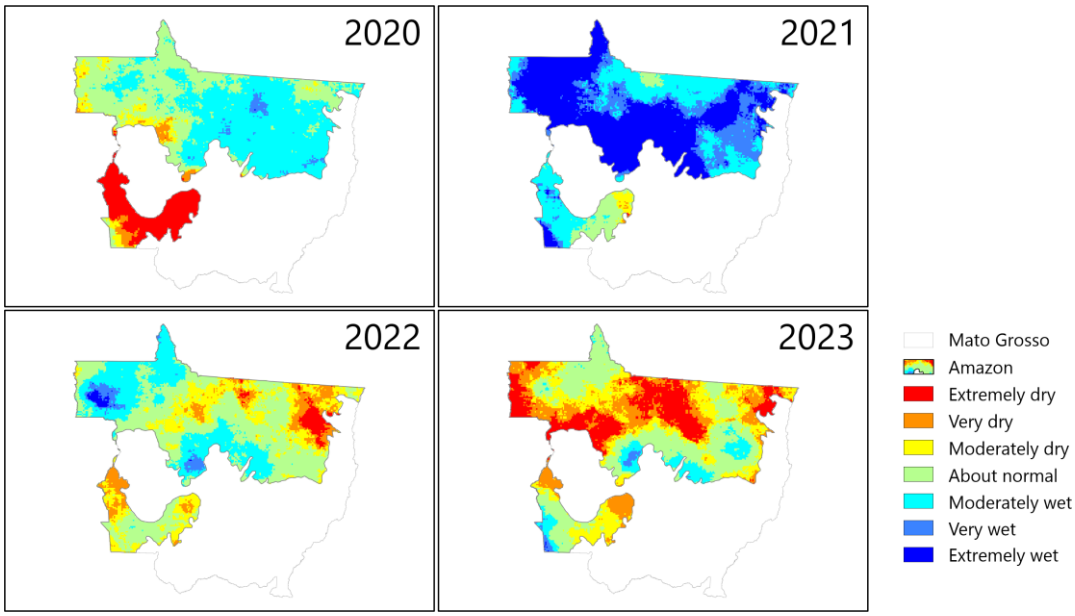

Figure 6. Standardized Precipitation Index (SPI) over Mato Grosso Amazon from 2020 to 2023. The spatialization of drought is based on the precipitation time series, considering the temporal periodicity; here, it was considered the annual index (SPI-12), i.e., the cumulated precipitation of each year was considered in modeling drought.

3.3. Temporal Trends of Orbital Carbon and Drought (2008–2023)

Results indicate distinct patterns in the variables analyzed (Table 1). For the SPI (Standardized Precipitation Index—Figure 6), the Mann–Kendall test did not reveal a significant trend ($S = 16$, $p = 0.4995$). The Pettitt test (U = 32) pointed to a potentially significant abrupt change, possibly associated with changes in precipitation regimes. Even though, the *p*-value for SPI is far from significant.

Table 1. Pettitt and Mann–Kendall tests for CO_2Flux, GPP and SPI temporality from 2008 to 2023.

	CO_2Flux	**GPP**	**SPI**
Pettitt			
U statistics	−44	−32	32
Critical value ($\alpha = 0.05$)	62.4	62.4	62.4
Change point	2013 (index 5)	2019 (index 11)	2011 (index 3)
p-value	0.0693	0.2437	0.2437
Mann–Kendall			
S statistics	−20	−10	16

S variance	493.33	493.33	493.33
Z statistics	−0.8554	−0.4052	0.6753
p-value	0.3923	0.6853	0.4995

Significance at 5%.

Finally, CO_2Flux showed marginal stability (S = −20, p = 0.0693—Table 1), with values becoming more negative over time in the perspective of time series (Figure 7). The Pettitt test (U = 17) did not indicate an abrupt change, which does not translate the global perspective of land use dynamics, as it comes to changes in vegetation or soil management. The combination of higher moisture (reflected in the form of SPI) and lower productivity (GPP — Figure 7) suggests that other factors, such as plant composition or ecosystem dynamics, may be influencing the carbon balance. These findings highlight the complexity of climate–vegetation–carbon interactions, especially in tropical ecosystems.

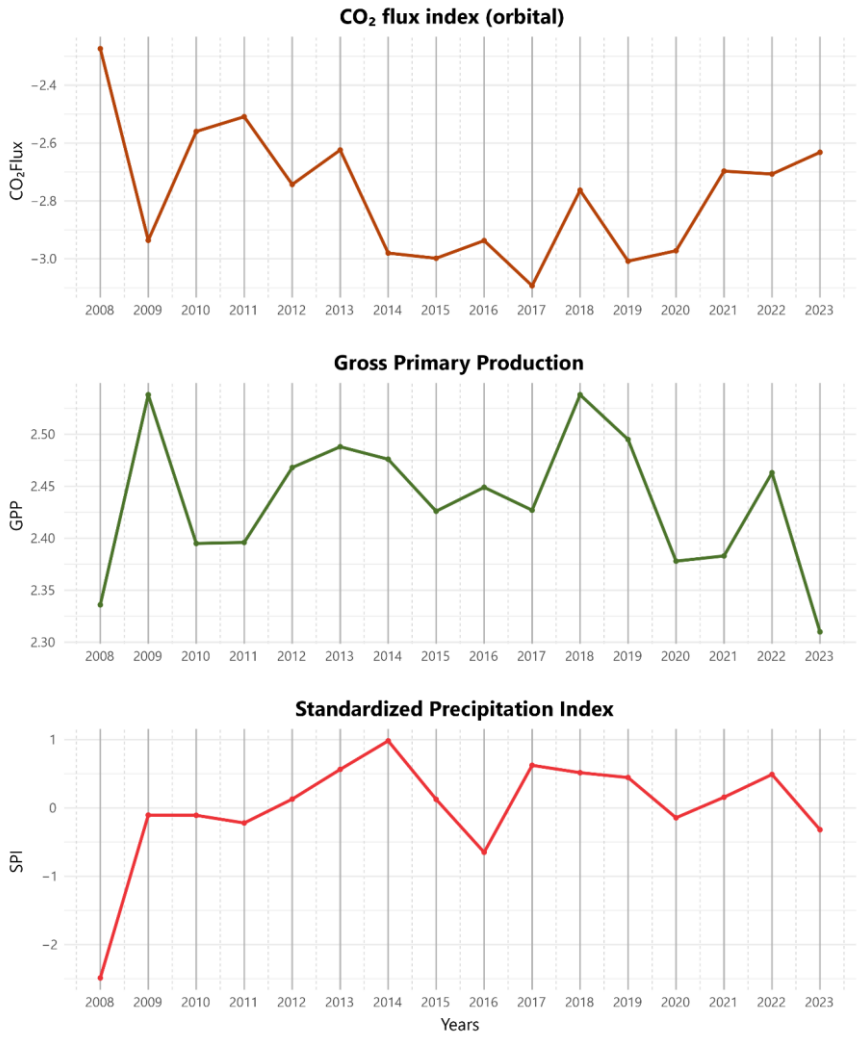

Figure 7. Averages of CO_2Flux [μmol m^{-2} s^{-1}], annual cumulated GPP [kg C m^{-2}], and Standardized Precipitation Index (SPI) for Mato Grosso Amazon from 2008 to 2023.

3.4. Hot and Cold Spots

Based on Getis-Ord Gi* statistics (Equation (25)), areas with higher amplitudes of the CO_2Flux, GPP, and SPI-12 variables were spatially highlighted. Using the "Find High Incidence Values" tool, patterns of higher and lower intensity were calculated for these carbon and orbital acquisition drought variables. For the orbital carbon variables, i.e.,

CO_2Flux (Figure 8) and GPP (Figure 9), some correlation is expected and reinforced by this approach. In addition, there is a notable correlation between both orbital carbon variables and the agricultural cultivation area, while on the other hand, they are not closely related to recent deforestation, based on PRODES deforestation data. The correlation between CO_2Flux and GPP goes beyond this simple correlation of variables and contributes to the premise, which is continuously being investigated [25], where the dynamics between atmospheric and soil carbon stocks depend on land use.

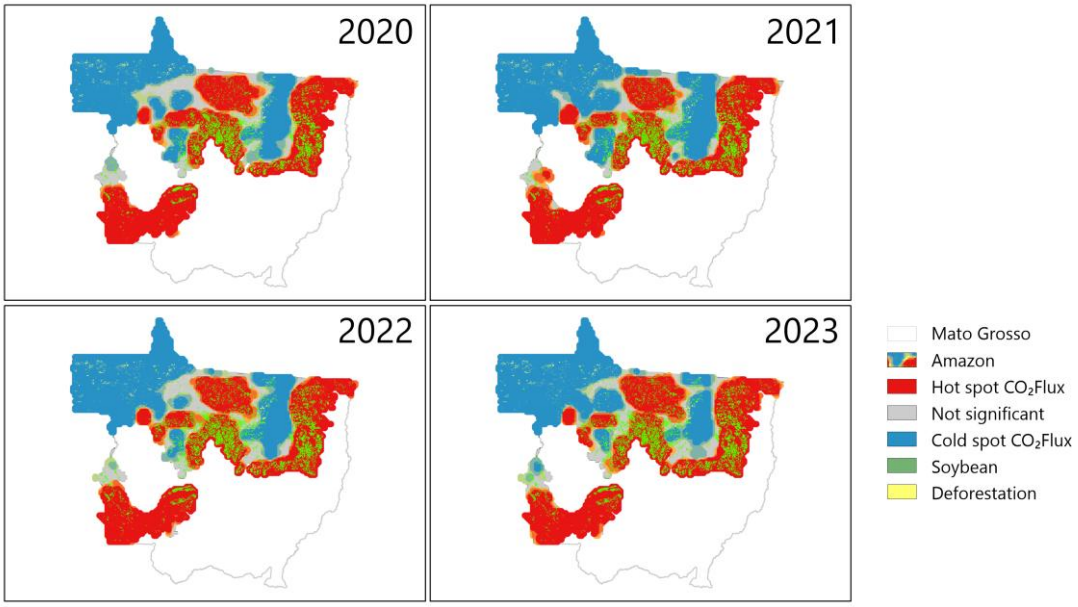

Figure 8. Annual average carbon dioxide flux (CO_2Flux) hot and cold spots for Mato Grosso Amazon from 2020 to 2023.

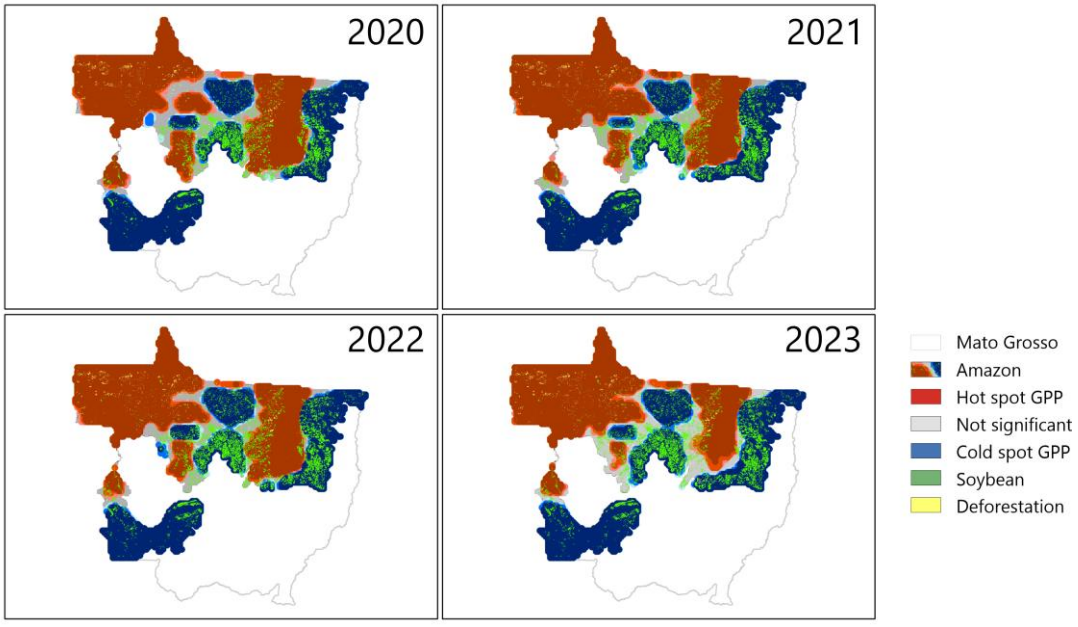

Figure 9. Annual average gross primary production (GPP) hot and cold spots for Mato Grosso Amazon from 2020 to 2023.

The cluster analysis of the drought index reveals a spatial effect on areas with changes in land cover. Following the method used to analyze the annual drought severity index for the crop years under analysis (2020 to 2023), it is possible to note the significance and

impact that soybean areas have on the determination of dry zones (Figure 10). Throughout the crop years studied, the north-central regions of the state of Mato Grosso (and the southern limit of the Amazon biome) and the far north region retained their hotspot characteristics, which, in the first example, suggests the prolonged effect of agricultural occupation on precipitation, as well as suggesting that areas undergoing expansion also determine the effect of drought.

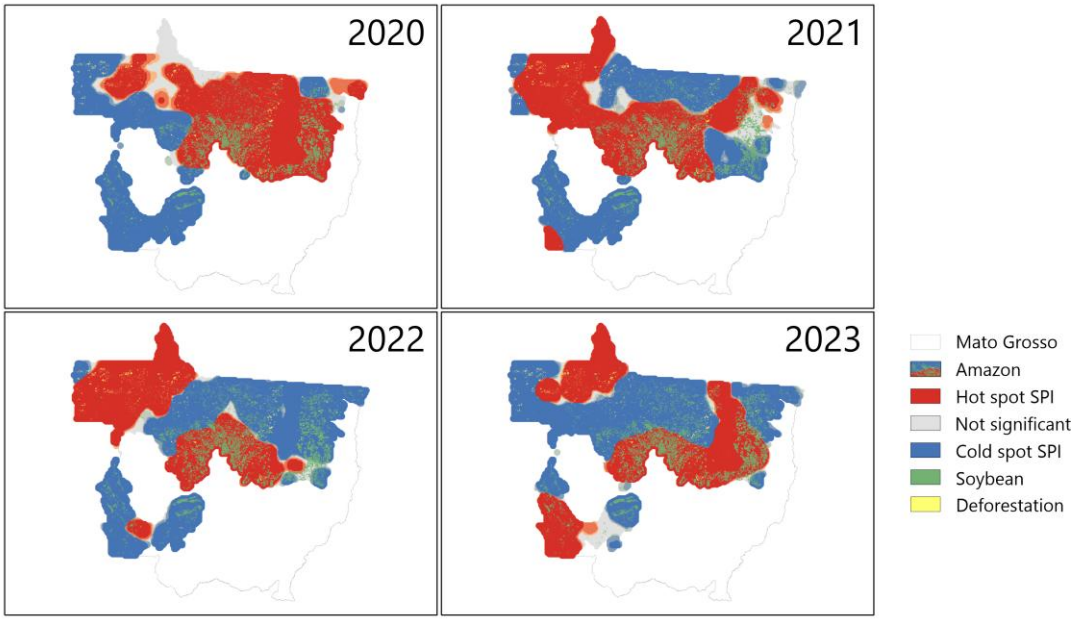

Figure 10. Annual Standardized Precipitation Index (SPI) hot and cold spots for Mato Grosso Amazon from 2020 to 2023. Hot spots of drought (in red) match the main soybean cultivation areas, in the north-central region of Mato Grosso.

The potential correlation between severe land use change dynamics and future effects is still apparent. For example, near the edge of the Pantanal, a hotspot area was identified after severe deforestation events, based on the use of fire for this process, which occurred in the previous year. The other areas that transition between dry and non-dry zoning are boundaries between large areas that remain dry or wet.

4. Discussion

Land use dynamics and their impact on carbon and water cycles are associated with the ecosystem structure established by each type of occupation. Commonly, the expansion of arable land is associated with deforestation, which in context means a decrease in evapotranspiration and soil organic carbon (SOC) stocks [63]. Despite this, the southern Amazon has a more complex dynamic of anthropization and agricultural productivity, where degraded pastureland is being replaced by soybean and corn fields, which increases biotic and soil carbon stocks. Consequently, evapotranspiration [64,65] and other related variables (soil microbiology, organic carbon, moisture, and temperature) are positively altered [66–68].

The spatialization of climate diagnostics for carbon and water cycles, and geographic diagnostics for dynamic land use, guides conclusions about the importance of the southern Amazon. The region's ecosystem services and the spatial intersection with the agricultural frontier of a country economically structured around agriculture, in addition to being the fourth largest agricultural producer in the world [69] converge environment and economy, highlighting the environmental commitment of the productive sector. This is an

anthropization process of a biodiversity hotspot on the planet, with the greatest potential for bioprospecting and the development of technologies from Brazilian biomes [70–72].

The relation (and, to a certain extent, dependence) between soybean productivity and drought highlights the need to keep the forest standing, to maintain the high productive capacity of this commodity. In a context where the largest soybean producer has an economy based on its export, conservation and development of productive capacity and increasing global exports are fundamental to meeting the Brazilian economic needs itself and the consumers' food security [73–75].

The value of Brazilian environmental concern policies as the soy moratorium [76], is foundational to restraining the deforestation for agricultural activities [3]. The spatialization of SPI (Figure 10) raises the limitation of the climatic influence of such a device, where previous land use dynamics of anthropization and natural climatic processes, such as El Niño, are prevailing on drought, and anything else that comes with it [36]. More than placing legal mechanisms for environmental concerns, it is necessary to define tools that effectively stop deforestation [77].

The results about drought (Figure 6), allied to the region Köppen–Geiger classifications ("Am"—monsoon climate, and "Aw/As"—tropical climate with dry season) expresses how anthropization affects the water cycles. In the region, extremely dry regions suffer the most from shortening of the rainy season, with more intense rainfall events [78,79]. Our results are based on remote sensing techniques, and the geochemical cycles models provide some estimated metrics, even though the spatialization of data, the data temporality, and the geoprocessing techniques in our methods, allied to an adequate statistical approach, ground the reliability of such findings.

The climate regulation of native forests, in terms of evapotranspiration, is related to land use [80]. Somehow, very large areas of cultivation mean massive losses of forest and the high evapotranspiration capacity it provides [81]. Given the estimated expansion of soybean cultivation into forest and pasture areas, consideration should be given to adopting farming systems that conserve more forests. In addition to this technical increase in commodity productivity, this also means conservation of species, natural capital, and other ecosystem services provided by the forest [82–85]. Beyond making use of unproductive areas, strategic planning and the agricultural production chain regulation are shaping the agricultural industry, where productivity and carbon absorption must be improved to positively impact the regional climate.

5. Conclusions

Remote sensing reaffirms the Amazon preservation importance for Brazil's agricultural sector. Economic and environmental synthesis outlooks reinforce attention to managing the biome's resources. Combined methodologies based on orbital data and climatology form the technical diagnosis for ecological treatment, necessary to adapt relations of humans and nature. The extreme hydrological cycle mainly affects the regional climate in the southern Amazon, but it also affects soybean productivity and the economic consequences of this lower productivity.

From a technical standpoint, spatial analysis will obviously be optimized with accurate models for biogeochemical agents. Regionalized analysis is highly dependent on land use, and therefore, we estimate that increasing the spatial resolution of products for rainfall (or drought) and carbon dioxide will also allow for more refined diagnoses. However, future results should be very similar, as the effects of anthropization on the climate are felt and observed globally. Economic planning and resource management embrace Amazon's soybean production. Even with formal planning and policies, further scientific progress on climate research, agricultural technology breakthroughs and natural resources

knowledge may lead to a sustainable economy, environmental commitment and food safe prospective.

Author Contributions: Conceptualization, C.A.d.S.J. and J.L.D.-S.; methodology, C.A.d.S.J., F.S.R. and J.L.D.-S.; software, C.A.d.S.J., F.S.R. and J.L.D.-S.; validation, J.L.D.-S., T.D.P. and W.B.M.; formal analysis, C.A.d.S.J. and J.L.D.-S.; investigation, J.L.D.-S.; resources, C.A.d.S.J.; data curation, C.A.d.S.J., F.S.R., and J.L.D.-S.; writing—original draft preparation, J.L.D.-S.; writing—review and editing, P.E.T. and L.P.R.T.; visualization, T.D.P. and W.B.M.; supervision, C.A.d.S.J., P.E.T., L.P.R.T. and D.A.; project administration, C.A.d.S.J.; funding acquisition, C.A.d.S.J. All authors have read and agreed to the published version of the manuscript.

Funding: This research was funded by Coordenação de Aperfeiçoamento de Pessoal de Nível Superior—Brasil (CAPES)—Finance Code 001, National Council for Research and Development (CNPq), Grant numbers 309250/2021-8 and 303767/2020-0.

Data Availability Statement: The data presented in this study are available in the article. More information is available on request from the corresponding authors.

Acknowledgments: We thank the research laboratories of State University of Mato Grosso (UNEMAT), Federal University of Mato Grosso do Sul (UFMS) and Centre National de la Recherche Scientifique, at Université Rennes 2. This research is derived from the first author's degree in the Graduate Program in Biodiversity and Biotechnology (PPG-Bionorte) at State University of Mato Grosso (UNEMAT).

Conflicts of Interest: The authors declare no conflicts of interest.

Abbreviations

The following abbreviations are used in this manuscript:

SPI	Standardized Precipitation Index
CO_2	Carbon dioxide
PCEI	Perpendicular Crop Enhancement Index
PVI	Perpendicular Vegetation Index
NIR	Near-infrared
NDFI	Normalized Difference Fraction Index
LSU	Linear Spectral Unmixing
MSE	Mean Squared Error
GV	Green vegetation
NPV	Non-photosynthetic vegetation
GV_{shade}	Shade-normalized GV fraction
GPP	Gross Primary Production
APAR	Absorbed photosynthetically active radiation
PAR	Photosynthetically active radiation
FPAR	Fraction of photosynthetically active radiation absorbed by the vegetation cover
VPD	Water vapor pressure deficit
NDVI	Normalized difference vegetation index
PRI	Photochemical reflectance index
sPRI	Scaled photochemical reflectance index
FCO_2	Soil carbon dioxide efflux
PDF	Probability Density Function
MLM	Maximum likelihood method
IDW	Inverse Distance Weighting
FDR	False discovery rate
SOC	Soil organic carbon

References

1. Escher, F.; Wilkinson, J. A Economia Política Do Complexo Soja-Carne Brasil-China. *Rev. Econ. Sociol. Rural.* **2019**, *57*, 656–678. https://doi.org/10.1590/1806-9479.2019.191017.
2. USDA. *World Agricultural Supply and Demand Estimates*; United States Department of Agriculture: Washington, DC, USA, 2024.
3. Kastens, J.H.; Brown, J.C.; Coutinho, A.C.; Bishop, C.R.; Esquerdo, J.C.D.M. Soy Moratorium Impacts on Soybean and Deforestation Dynamics in Mato Grosso, Brazil. *PLoS ONE* **2017**, *12*, e0176168. https://doi.org/10.1371/journal.pone.0176168.
4. Chaves, M.E.D.; Alves, M.d.C. Recent Applications of the MODIS Sensor for Soybean Crop Monitoring and Deforestation Detection in Mato Grosso, Brazil. *CAB Rev. Perspect. Agric. Vet. Sci. Nutr. Nat. Resour.* **2019**, *14*, 1–9.
5. Gollnow, F.; Hissa, L.d.B.V.; Rufin, P.; Lakes, T. Property-Level Direct and Indirect Deforestation for Soybean Production in the Amazon Region of Mato Grosso, Brazil. *Land Use Policy* **2018**, *78*, 377–385. https://doi.org/10.1016/j.landusepol.2018.07.010.
6. Marin, F.R.; Zanon, A.J.; Monzon, J.P.; Andrade, J.F.; Silva, E.H.F.M.; Richter, G.L.; Antolin, L.A.S.; Ribeiro, B.S.M.R.; Ribas, G.G.; Battisti, R.; et al. Protecting the Amazon Forest and Reducing Global Warming via Agricultural Intensification. *Nat. Sustain.* **2022**, *5*, 1018–1026. https://doi.org/10.1038/s41893-022-00968-8.
7. Abdala, L.J.; Otegui, M.E.; Di Mauro, G. On-Farm Soybean Genetic Progress and Yield Stability during the Early 21st Century: A Case Study of a Commercial Breeding Program in Argentina and Brazil. *Field Crops Res.* **2024**, *308*, 109277. https://doi.org/10.1016/j.fcr.2024.109277.
8. Todeschini, M.H.; Milioli, A.S.; Rosa, A.C.; Dallacorte, L.V.; Panho, M.C.; Marchese, J.A.; Benin, G. Soybean Genetic Progress in South Brazil: Physiological, Phenological and Agronomic Traits. *Euphytica* **2019**, *215*, 124. https://doi.org/10.1007/s10681-019-2439-9.
9. Noack, F.; Engist, D.; Gantois, J.; Gaur, V.; Hyjazie, B.F.; Larsen, A.; M'Gonigle, L.K.; Missirian, A.; Qaim, M.; Sargent, R.D.; et al. Environmental Impacts of Genetically Modified Crops. *Science* **2024**, *385*, eado9340.
10. Koiffmann Becker, B. Novas Territorialidades Na Amazônia: Desafio Às Políticas Públicas. *Bol. Mus. Para. Emílio Goeldi. Ciências Humanas* **2010**, *5*, 17–23.
11. Homma, A.K.O. Evolução Histórica dos Macrossistemas de Produção Na Amazônia. In *Encontro da Sociedade Brasileira de Sistemas de Produção*; UFPA: Embrapa Amazônia Oriental: Belém, Brazil, 2001.
12. Canavarros, O.; Peraro, M.A.; Borges, F.T.d.M.; Joanoni Neto, V. Mato Grosso Nos Estudos Historiográficos. *Rev. Territ. Front.* **2012**, *5*, 79–97.
13. Murtinho, M.N. Análise Econômica da Divisão de Mato Grosso (1970–2000). Master's Thesis, UFMT: Cuiabá, Brazil, 2009.
14. Campos, M.S.; Anjos, L.J.S.; Souza, E.B.d.; Bezerra, F.G.S.; Lima, A.M.M.d.; Galbraith, D.R.; Adami, M. Prioritizing Amazon Forest Conservation: Assessing Potential Biomass under Climate Change. *Glob. Ecol. Conserv.* **2024**, *54*, e03106. https://doi.org/10.1016/j.gecco.2024.e03106.
15. Costa, J.R.d.; Colares, L.M.L.; Monteiro, G.R. Caracterização Da Flora e Da Fauna Em Estudo Ambiental Simplificado Na Amazônia Central. *Rev. Biodiversidade* **2022**, *21*, 72–88.
16. Moraes, B.C.d.; Sodré, G.R.C.; Ferreira, H.d.S.; Silva, C.N.d.; Ribeiro, J.B.M.; Silva Júnior, J.d.A.; Rodrigues, M.S.; Lima, J.B.M.d.; Monteiro, T.M.C.; Figueiredo, F.M. Impacto Das Alterações Climáticas Na Amazônia Oriental: O Avanço Da Seca Na Região Agrícola Do Sudeste Paraense. In *Amazônia: Tópicos Atuais em Ambiente, Saúde e Educação*; Santos, D.M.A., Viana, W.C., Eds.; Científica Digital: Guarujá, Brazil, 2024; Volume 5, pp. 257–282, ISBN 978-65-5360-580-0.
17. Nobre, A.D. *The Future Climate of Amazonia*; ARA: CCST-INPE: INPA, Brazil, 2014.
18. Alvares, C.A.; Stape, J.L.; Sentelhas, P.C.; Gonçalves, J.L.d.M.; Sparovek, G. Köppen's Climate Classification Map for Brazil. *Meteorol. Z.* **2013**, *22*, 711–728.
19. Chaves de Oliveira, E. Balanço de Carbono e Energia Para Uma Lavoura de Soja: Método da Covariância dos Vórtices Turbulentos e a Estimativa do Modelo CROPGRO-Soybean. Ph.D. Thesis, Universidade Federal de Viçosa: Viçosa, Brazil, 2011.
20. Batista, F.d.S.; Duku, C.; Hein, L. Deforestation-Induced Changes in Rainfall Decrease Soybean-Maize Yields in Brazil. *Ecol. Modell.* **2023**, *486*, 110533. https://doi.org/10.1016/j.ecolmodel.2023.110533.
21. Vieira Filho, J.E.R. A Produção de Soja e Sua Importância Na Economia Brasileira. *Rev. Política Agrícola* **2024**, *33*, e01962. https://doi.org/10.35977/2317-224X.
22. Gurgel, A.C.; Seabra, J.E.A.; Arantes, S.M.; Moreira, M.M.R.; Lynd, L.R.; Galindo, R. Contribution of Double-Cropped Maize Ethanol in Brazil to Sustainable Development. *Nat. Sustain.* **2024**, *7*, 1429–1440. https://doi.org/10.1038/s41893-024-01424-5.

23. Chen, M.; Samat, N.; Maghsoodi Tilaki, M.J.; Duan, L. Land Use/Cover Change Simulation Research: A System Literature Review Based on Bibliometric Analyses. *Ecol. Indic.* **2025**, *170*, 112991. https://doi.org/10.1016/j.ecolind.2024.112991.
24. Yue, F.; Liu, D.; Xiong, L.; Chen, J.; Chen, H.; Yin, J. Understanding the Roles of Climate Change, Land Use and Land Cover Change and Water Diversion Project in Modulating Water- and Carbon-Use Efficiency in Han River Basin. *J. Environ. Manag.* **2025**, *373*, 123445. https://doi.org/10.1016/j.jenvman.2024.123445.
25. Della-Silva, J.L.; da Silva Junior, C.A.; Lima, M.; Teodoro, P.E.; Nanni, M.R.; Shiratsuchi, L.S.; Teodoro, L.P.; Capristo-Silva, G.F.; Baio, F.H.; de Oliveira, G.; et al. CO_2Flux Model Assessment and Comparison between an Airborne Hyperspectral Sensor and Orbital Multispectral Imagery in Southern Amazonia. *Sustainability* **2022**, *14*, 5458. https://doi.org/10.3390/su14095458.
26. Della-Silva, J.L.; Lima, M.; Teodoro, L.P.R.; Crusiol, L.G.T.; La Scala, N.; Rossi, F.S.; Arvor, D.; Teodoro, P.E.; Silva Junior, C.A.d. Modeling Orbital Data of Soil Carbon Dioxide Efflux from Different Land Uses in Southern Amazon. *J. S. Am. Earth Sci.* **2025**, *152*, 105323. https://doi.org/10.1016/j.jsames.2024.105323.
27. Rossi, F.S.; La Scala, N.; Capristo-Silva, G.F.; Della-Silva, J.L.; Teodoro, L.P.R.; Almeida, G.; Tiago, A.V.; Teodoro, P.E.; Silva Junior, C.A.d. Implications of CO2 Emissions on the Main Land and Forest Uses in the Brazilian Amazon. *Environ. Res.* **2023**, *227*, 115729. https://doi.org/10.1016/j.envres.2023.115729.
28. Silva, B.C.d.; Prado, R.d.M.; Baio, F.H.R.; Campos, C.N.S.; Teodoro, L.P.R.; Teodoro, P.E.; Santana, D.C.; Fernandes, T.F.S.; Silva Junior, C.A.d.; Loureiro, E.d.S. New Approach for Predicting Nitrogen and Pigments in Maize from Hyperspectral Data and Machine Learning Models. *Remote Sens. Appl.* **2024**, *33*, 101110. https://doi.org/10.1016/j.rsase.2023.101110.
29. El Azizi, S.; Amharref, M.; Es-Saouini, H.; Bernoussi, A.-S.; El Abdellaoui, J.E. Towards a Spectral Library of Medicinal and Aromatic Plant Species (MAPs): Plant Discrimination and Wavelength Selection. *Microchem. J.* **2024**, *207*, 111854. https://doi.org/10.1016/j.microc.2024.111854.
30. Teodoro, P.E.; Rossi, F.S.; Teodoro, L.P.R.; Santana, D.C.; Ratke, R.F.; Oliveira, I.C.d.; Della Silva, J.L.; Oliveira, J.L.G.d.; Silva, N.P.d.; Baio, F.H.R.; et al. Soil CO_2 Emissions under Different Land-Use Managements in Mato Grosso Do Sul, Brazil. *J. Clean. Prod.* **2024**, *434*, 139983. https://doi.org/10.1016/j.jclepro.2023.139983.
31. Almagro, M.; López, J.; Querejeta, J.I.; Martínez-Mena, M. Temperature Dependence of Soil CO_2 Efflux Is Strongly Modulated by Seasonal Patterns of Moisture Availability in a Mediterranean Ecosystem. *Soil Biol. Biochem.* **2009**, *41*, 594–605. https://doi.org/10.1016/j.soilbio.2008.12.021.
32. Rao, K.; Sarma, D.; Deb Burman, P.K.; Agarwal, G.; Datye, A.; Tiwari, Y.K.; Gogoi, N. Subtropical Forest Floor CO2 Emission at the Kaziranga National Park in Northeast India. *Environ. Monit. Assess.* **2025**, *197*, 133. https://doi.org/10.1007/s10661-024-13586-y.
33. Medeiros, A.d.S.; Cesário, F.V.; Santos, T.C.d.; Ferreira Maia, S.M. Differences in the Storage of Soil Organic Carbon in Brazil's Agricultural Land: A Meta-Analysis. *Catena* **2025**, *249*, 108680. https://doi.org/10.1016/j.catena.2024.108680.
34. Monteiro, A.; Barreto-Mendes, L.; Fanchone, A.; Morgavi, D.P.; Pedreira, B.C.; Magalhães, C.A.S.; Abdalla, A.L.; Eugène, M. Crop-Livestock-Forestry Systems as a Strategy for Mitigating Greenhouse Gas Emissions and Enhancing the Sustainability of Forage-Based Livestock Systems in the Amazon Biome. *Sci. Total Environ.* **2024**, *906*, 167396. https://doi.org/10.1016/j.scitotenv.2023.167396.
35. Gonçalves e Silva, J.A.; Habermann, E.; de Pinho Costa, K.A.; da Silva, L.M.; da Costa Severiano, E.; Costa, A.C.; Silva, F.G.; de Oliveira, T.C.; Dário, B.M.M.; Vilela, L.; et al. Integration Crop-Livestock System Increases the Sustainability of Soybean Cultivation through Improved Soil Health and Plant Physiology. *Agric. Ecosyst. Environ.* **2024**, *359*, 108770. https://doi.org/10.1016/j.agee.2023.108770.
36. Rossi, F.S.; de Araújo Santos, G.A.; de Souza Maria, L.; Lourençoni, T.; Pelissari, T.D.; Della-Silva, J.L.; Júnior, J.W.O.; de Avila e Silva, A.; Lima, M.; Teodoro, P.E.; et al. Carbon Dioxide Spatial Variability and Dynamics for Contrasting Land Uses in Central Brazil Agricultural Frontier from Remote Sensing Data. *J. S. Am. Earth Sci.* **2022**, *116*, 103809. https://doi.org/10.1016/j.jsames.2022.103809.
37. Crivelari-Costa, P.M.; Lima, M.; La Scala, N., Jr.; Rossi, F.S.; Della-Silva, J.L.; Dalagnol, R.; Teodoro, P.E.; Teodoro, L.P.R.; Oliveira, G.d.; Junior, J.F.d.O.; et al. Changes in Carbon Dioxide Balance Associated with Land Use and Land Cover in Brazilian Legal Amazon Based on Remotely Sensed Imagery. *Remote Sens.* **2023**, *15*, 2780. https://doi.org/10.3390/rs15112780.
38. Pretty, J. Intensification for Redesigned and Sustainable Agricultural Systems. *Science* **2018**, *362*, eaav0294. https://doi.org/10.1126/science.aav0294.
39. Gorelick, N.; Hancher, M.; Dixon, M.; Ilyushchenko, S.; Thau, D.; Moore, R. Google Earth Engine: Planetary-Scale Geospatial Analysis for Everyone. *Remote Sens. Environ.* **2017**, *202*, 18–27. https://doi.org/10.1016/J.RSE.2017.06.031.

40. SOJAMAPS Monitoramento de Áreas de Soja Por Meio de Imagens de Satélite. Availabe online: https://pesquisa.unemat.br/gaaf/plataformas/ (accessed on 10 October 2021).
41. da Silva Junior, C.A.; Nanni, M.R.; Teodoro, P.E.; Silva, G.F.C. Vegetation Indices for Discrimination of Soybean Areas: A New Approach. *Agron. J.* **2017**, *109*, 1331–1343. https://doi.org/10.2134/agronj2017.01.0003.
42. Souza Junior, C.M.; Roberts, D.A.; Cochrane, M.A. Combining Spectral and Spatial Information to Map Canopy Damage from Selective Logging and Forest Fires. *Remote Sens. Environ.* **2005**, *98*, 329–343. https://doi.org/10.1016/j.rse.2005.07.013.
43. Shimabukuro, Y.E.; Smith, J.A. The Least-Squares Mixing Models to Generate Fraction Images Derived from Remote Sensing Multispectral Data. *IEEE Trans. Geosci. Remote Sens.* **1991**, *29*, 16–20. https://doi.org/10.1109/36.103288.
44. Souza-Junior, C.M.d.; Siqueira, J.; Sales, M.; Fonseca, A.; Ribeiro, J.; Numata, I.; Cochrane, M.; Barber, C.; Roberts, D.; Barlow, J. Ten-Year Landsat Classification of Deforestation and Forest Degradation in the Brazilian Amazon. *Remote Sens.* **2013**, *5*, 5493–5513. https://doi.org/10.3390/rs5115493.
45. Didan, K.; Munoz, A.B.; Solano, R.; Huete, A. *MODIS Vegetation Index User 's Guide*; Collection 6; NASA: Washington, DC, USA, 2015; Volume 2013, p. 31.
46. Rahman, A.F.; Gamon, J.A.; Fuentes, D.A.; Roberts, D.A.; Prentiss, D. Modeling Spatially Distributed Ecosystem Flux of Boreal Forest Using Hyperspectral Indices from AVIRIS Imagery. *J. Geophys. Res. Atmos.* **2001**, *106*, 33579–33591. https://doi.org/10.1029/2001jd900157.
47. Santos, C.V.B.d. Modelagem Espectral Para Determinação de Fluxo de CO_2 em Áreas de Caatinga Preservada e em Regeneração. Master's Thesis, Universidade Estadual de Feira de Santana: Feira de Santana, Brazil, 2017.
48. Field, C.B.; Randerson, J.T.; Malmström, C.M. Global Net Primary Production: Combining Ecology and Remote Sensing. *Remote Sens. Environ.* **1995**, *51*, 74–88. https://doi.org/10.1016/0034-4257(94)00066-V.
49. Running, S.W.; Zhao, M. *MOD17A2H MODIS/Terra Gross Primary Productivity 8-Day L4 Global 500m SIN Grid V006*; NASA EOSDIS Land Processes Distributed Active Archive Center: Washington, DC, USA, 2015.
50. Wan, Z.; Hook, S.; Hulley, G. MODIS/Terra Land Surface Temperature/Emissivity Daily L3 1km SIN Grid V061 2021.
51. Chan, S.K.; Bindlish, R.; O'Neill, P.E.; Njoku, E.; Jackson, T.; Colliander, A.; Chen, F.; Burgin, M.; Dunbar, S.; Piepmeier, J.; et al. Assessment of the SMAP Passive Soil Moisture Product. *IEEE Trans. Geosci. Remote Sens.* **2016**, *54*, 4994–5007. https://doi.org/10.1109/TGRS.2016.2561938.
52. Chan, S.K.; Bindlish, R.; O'Neill, P.; Jackson, T.; Njoku, E.; Dunbar, S.; Chaubell, J.; Piepmeier, J.; Yueh, S.; Entekhabi, D.; et al. Development and Assessment of the SMAP Enhanced Passive Soil Moisture Product. *Remote Sens. Environ.* **2018**, *204*, 931–941. https://doi.org/10.1016/j.rse.2017.08.025.
53. Chaubell, M.J.; Yueh, S.H.; Dunbar, R.S.; Colliander, A.; Chen, F.; Chan, S.K.; Entekhabi, D.; Bindlish, R.; O'Neill, P.E.; Asanuma, J.; et al. Improved SMAP Dual-Channel Algorithm for the Retrieval of Soil Moisture. *IEEE Trans. Geosci. Remote Sens.* **2020**, *58*, 3894–3905. https://doi.org/10.1109/TGRS.2019.2959239.
54. McKee, T.B.; Doesken, N.J.; Kleist, J. The Relationship of Drought Frequency and Duration to Time Scales. In Proceedings of the Eighth Conference on Applied Climatology, Anaheim, CA, USA, 17–22 January 1993; pp. 179–184.
55. Gois, G.D.; Souza, J.L.D. Caracterização da Desertificação No Estado de Alagoas Utilizando Variáveis Climáticas. *Rev. Bras. Meteorol.* **2005**, *20*, 301–314.
56. Climate Hazards Center, U.S.B. CHIRPS: Rainfall Estimates from Rain Gauge and Satellite Observations Available online: https://www.chc.ucsb.edu/data/chirps/ (accessed on 12 February 2025).
57. Knapp, K.R.; Ansari, S.; Bain, C.L.; Bourassa, M.A.; Dickinson, M.J.; Funk, C.; Helms, C.N.; Hennon, C.C.; Holmes, C.D.; Huffman, G.J.; et al. Globally Gridded Satellite Observations for Climate Studies. *Bull. Am. Meteorol. Soc.* **2011**, *92*, 893–907. https://doi.org/10.1175/2011BAMS3039.1.
58. Saha, S.; Moorthi, S.; Pan, H.-L.; Wu, X.; Wang, J.; Nadiga, S.; Tripp, P.; Kistler, R.; Woollen, J.; Behringer, D.; et al. The NCEP Climate Forecast System Reanalysis. *Bull. Am. Meteorol. Soc.* **2010**, *91*, 1015–1058. https://doi.org/10.1175/2010BAMS3001.1.
59. Toté, C.; Patricio, D.; Boogaard, H.; der Wijngaart, R.; Tarnavsky, E.; Funk, C. Evaluation of Satellite Rainfall Estimates for Drought and Flood Monitoring in Mozambique. *Remote Sens.* **2015**, *7*, 1758–1776. https://doi.org/10.3390/rs70201758.
60. Funk, C.C.; Peterson, P.J.; Landsfeld, M.F.; Pedreros, D.H.; Verdin, J.P.; Rowland, J.D.; Romero, B.E.; Husak, G.J.; Michaelsen, J.C.; Verdin, A.P.; et al. *A Quasi-Global Precipitation Time Series for Drought Monitoring*; The US Geological Survey: Reston, VA, USA, 2014.
61. Duan, Z.; Liu, J.; Tuo, Y.; Chiogna, G.; Disse, M. Evaluation of Eight High Spatial Resolution Gridded Precipitation Products in Adige Basin (Italy) at Multiple Temporal and Spatial Scales. *Sci. Total Environ.* **2016**, *573*, 1536–1553. https://doi.org/10.1016/j.scitotenv.2016.08.213.

62. Getis, A.; Ord, J.K. The Analysis of Spatial Association by Use of Distance Statistics. *Geogr. Anal.* **1992**, *24*, 189–206. https://doi.org/10.1111/j.1538-4632.1992.tb00261.x.
63. Sun, J.; Twine, T.E.; Hill, J.; Noe, R.; Shi, J.; Li, M. Effects of Land Use Change for Crops on Water and Carbon Budgets in the Midwest USA. *Sustainability* **2017**, *9*, 225. https://doi.org/10.3390/su9020225.
64. de Area Leão Pereira, E.J.; de Santana Ribeiro, L.C.; da Silva Freitas, L.F.; de Barros Pereira, H.B. Brazilian Policy and Agribusiness Damage the Amazon Rainforest. *Land Use Policy* **2020**, *92*, 104491. https://doi.org/10.1016/j.landusepol.2020.104491.
65. Zoungrana, B.J.-B.; Conrad, C.; Amekudzi, L.K.; Thiel, M.; Da, E.D. Land Use/Cover Response to Rainfall Variability: A Comparing Analysis between NDVI and EVI in the Southwest of Burkina Faso. *Climate* **2015**, *3*, 63–77. https://doi.org/10.3390/cli3010063.
66. Bini, D.; Santos, C.A.d.; Carmo, K.B.d.; Kishino, N.; Andrade, G.; Zangaro, W.; Nogueira, M.A. Effects of Land Use on Soil Organic Carbon and Microbial Processes Associated with Soil Health in Southern Brazil. *Eur. J. Soil Biol.* **2013**, *55*, 117–123. https://doi.org/10.1016/j.ejsobi.2012.12.010.
67. Szoboszlay, M.; Dohrmann, A.B.; Poeplau, C.; Don, A.; Tebbe, C.C. Impact of Land-Use Change and Soil Organic Carbon Quality on Microbial Diversity in Soils across Europe. *FEMS Microbiol. Ecol.* **2017**, *93*, fix146. https://doi.org/10.1093/femsec/fix146.
68. Ferreira, A.C.C.; Leite, L.F.C.; de Araújo, A.S.F.; Eisenhauer, N. Land-Use Type Effects on Soil Organic Carbon and Microbial Properties in a Semi-Arid Region of Northeast Brazil. *Land Degrad. Dev.* **2016**, *27*, 171–178. https://doi.org/10.1002/ldr.2282.
69. FAO. *World Food and Agriculture—Statistical Yearbook*; FAO: Rome, Italy, 2024; Volume 2024, pp. 1–384.
70. de Macedo Klautau, A.G.C.; Cordeiro, A.P.B.; das Chagas, R.A.; dos Santos, W.C.R.; Marceniuk, A.P.; da Nóbrega, P.S.V.; Martinelli-Lemos, J.M.; Cintra, I.H.A.; de Castro, N.S.S.; Bastos, C.E.M.C.; et al. Biodiversity Hotspots and Threatened Species under Human Influence in the Amazon Continental Shelf. *Sci. Rep.* **2025**, *15*, 26681. https://doi.org/10.1038/s41598-025-11261-x.
71. Fearnside, P.M. The Intrinsic Value of Amazon Biodiversity. *Biodivers. Conserv.* **2021**, *30*, 1199–1202. https://doi.org/10.1007/s10531-021-02133-7.
72. Fernandes, A.M.; Teixeira, O.d.S.; Garcia, E.B.; Matos, M.L.C.; Matos, G.B.d.C.; Pazdiora, R.D. Biodiversidade Na Amazônia Brasileira: Prospecção Científica e Tecnológica. *Front. J. Soc. Technol. Environ. Sci.* **2025**, *14*, 225–245. https://doi.org/10.21664/2238-8869.2025v14i2.p225-245.
73. Dhoubhadel, S.P.; Ridley, W.; Devadoss, S. Brazilian Soybean Expansion, US–China Trade War, and US Soybean Exports. *J. Agric. Appl. Econ. Assoc.* **2023**, *2*, 446–460. https://doi.org/10.1002/jaa2.71.
74. Colussi, J.; Schnitkey, G.; Janzen, J.; Paulson, N. The United States, Brazil, and China Soybean Triangle: A 20-Year Analysis. *AgEcon Search Res. Agric. Appl. Econ.* **2024**, *14*, 1–4. https://doi.org/10.22004/ag.econ.358571.
75. Montanía, C.V.; Fernández-Núñez, T.; Márquez, M.A. The Role of the Leading Exporters in the Global Soybean Trade. *Agric. Econ.* **2021**, *67*, 277–285. https://doi.org/10.17221/433/2020-AGRICECON.
76. Gibbs, H.K.; Rausch, L.; Munger, J.; Schelly, I.; Morton, D.C.; Noojipady, P.; Soares-Filho, B.; Barreto, P.; Micol, L.; Walker, N.F. Environment and Development. Brazil's Soy Moratorium. *Science* **2015**, *347*, 377–378. https://doi.org/10.1126/science.aaa0181.
77. Silva Junior, C.A.d.; Lima, M. Soy Moratorium in Mato Grosso: Deforestation Undermines the Agreement. *Land Use Policy* **2018**, *71*, 540–542. https://doi.org/10.1016/j.landusepol.2017.11.011.
78. Silva, R.D.S.; Dallacort, R.; Junior, I.C.M.; Carvalho, M.A.C.D.; Yamashita, O.M.; Santana, D.C.; Teodoro, L.P.R.; Teodoro, P.E.; Junior, C.A.d.S. Rainfall and Extreme Drought Detection: An Analysis for a Potential Agricultural Region in the Southern Brazilian Amazon. *Sustainability* **2024**, *16*, 5959. https://doi.org/10.3390/SU16145959.
79. Grimm, A.M.; Tedeschi, R.G. ENSO and Extreme Rainfall Events in South America. *J. Clim.* **2009**, *22*, 1589–1609. https://doi.org/10.1175/2008JCLI2429.1.
80. Ma, N.; Szilagyi, J.; Zhang, Y. Calibration-Free Complementary Relationship Estimates Terrestrial Evapotranspiration Globally. *Water Resour. Res.* **2021**, *57*, e2021WR029691. https://doi.org/10.1029/2021WR029691.
81. Moura, M.M.; dos Santos, A.R.; Pezzopane, J.E.M.; Alexandre, R.S.; da Silva, S.F.; Pimentel, S.M.; de Andrade, M.S.S.; Silva, F.G.R.; Branco, E.R.F.; Moreira, T.R.; et al. Relation of El Niño and La Niña Phenomena to Precipitation, Evapotranspiration and Temperature in the Amazon Basin. *Sci. Total Environ.* **2019**, *651*, 1639–1651. https://doi.org/10.1016/j.scitotenv.2018.09.242.
82. de Araujo Fonseca, F.N.; da Cunha Bustamante, M.M. The Importance of Indigenous Territories for the Provision of Ecosystem Services: A Case Study in the Brazilian Cerrado-Amazon Transition. *Ecosyst. Serv.* **2025**, *72*, 101706. https://doi.org/10.1016/j.ecoser.2025.101706.
83. Tölgyesi, C.; Csikós, N.; Temperton, V.M.; Buisson, E.; Silveira, F.A.O.; Lehmann, C.E.R.; Török, P.; Bátori, Z.; Bede-Fazekas, Á. Limited Carbon Sequestration Potential from Global Ecosystem Restoration. *Nat. Geosci.* **2025**, *18*, 761–768. https://doi.org/10.1038/s41561-025-01742-z.

84. Strand, J.; Soares-Filho, B.; Costa, M.H.; Oliveira, U.; Ribeiro, S.C.; Pires, G.F.; Oliveira, A.; Rajão, R.; May, P.; van der Hoff, R.; et al. Spatially Explicit Valuation of the Brazilian Amazon Forest's Ecosystem Services. *Nat. Sustain.* **2018**, *1*, 657–664. https://doi.org/10.1038/s41893-018-0175-0.
85. Pavanelli, D.D.; Domingues, D.F.; Hoch, P.G.; Alves, R.d.A.L.; Bezerra, A.C.; Pereira, M.H.B.; Raupp, A.B.; Klotz, A.O.; Magliano, M.M. Economic Valuation of Illegal Brazilian Amazon Deforestation: A Framework Based on Habitat Equivalency Analysis and Ecosystem Services Restoration. *Forensic Sci. Int.* **2025**, *367*, 112307. https://doi.org/10.1016/j.forsciint.2024.112307.